Diagn Interv Radiol 2025; DOI: 10.4274/dir.2025.253640

ABDOMINAL IMAGING

ORIGINAL ARTICLE

Texture analysis enhances diagnostic accuracy of lesions scored as 5 in the Prostate Imaging Reporting and Data System in magnetic resonance imaging

Yan Bai[1,2,3]
Xin Ru Xie[3]
Ying Hou[1,3]
Yu Dong Zhang[1,3]
Hai Bin Shi[1,3*]
Chen Jiang Wu[1,3*]

[1]The First Affiliated Hospital with Nanjing Medical University, Department of Radiology, Nanjing, China

[2]The First Affiliated Hospital of Baotou Medical College, Inner Mongolia University of Science and Technology, Baotou, China

[3]School of Medical Imaging,Nanjing Medical University, Nanjing, China

* There authors contributed equally to this work

Corresponding author: Chen Jiang Wu

E-mail: njmu_wcj@163.com

Received 08 September 2025; revision requested 05 October 2025; accepted 08 November 2025.

PURPOSE

Prostatitis is frequently observed in false-positive lesions scored as 5 in the Prostate Imaging Reporting and Data System (PI-RADS), necessitating improved diagnostic tools. This study investigated the potential of magnetic resonance imaging (MRI) texture analysis of apparent diffusion coefficient (ADC) sequences to enhance the differentiation of prostatitis from prostate cancer (PCa) in PI-RADS 5 lesions.

METHODS

This retrospective study enrolled patients undergoing 3.0-T MRI with lesions scored as PI-RADS 5. Lesions were manually delineated on ADC maps, and texture features were extracted using FireVoxel. Clinical data and ADC texture parameters were collected. The diagnostic performance [area under the curve (AUC), sensitivity (SEN), specificity (SPE), positive predictive value (PPV), negative predictive value (NPV)] of the clinical data, ADC texture, and a combined model were calculated and compared using the DeLong test.

RESULTS

The final cohort included 189 patients with 189 PI-RADS 5 lesions (164 PCa, 25 prostatitis). The combined model, incorporating clinical indicators (age, prostate-specific antigen density) and ADC texture parameters (signal coefficient of variation, ADC percentile), revealed the optimal diagnostic performance: SEN 98.7%, SPE 60.0%, PPV 97.9%, NPV 71.6%, and AUC 93.1%. Bootstrap resampling verified the robustness of the model. Decision curve analysis indicated an improved net benefit with the combined model for guiding biopsy decisions.

CONCLUSION

ADC imaging texture parameters are valuable for the differential diagnosis of prostatitis from lesions scored as PI-RADS 5. Their combination with clinical indicators substantially improves diagnostic performance, providing valuable information to facilitate surgical decision-making and potentially reduce unnecessary biopsies.

CLINICAL SIGNIFICANCE

This study addresses a critical limitation of the current PI-RADS system, which exhibits a notable rate of false positives in high-risk PI-RADS 5 lesions. By demonstrating the added value of quantitative ADC texture analysis in this specific diagnostic challenge, this research offers a practical and potentially translatable approach to reducing the number of unnecessary biopsies for PI-RADS 5 lesions.

KEYWORDS

Prostate cancer, prostatitis, PI-RADS 5, magnetic resonance imaging, diffusion-weighted imaging, apparent diffusion coefficient, texture analysis, differential diagnosis

Epub: 01.12.2025

DOI: 10.4274/dir.2025.253640

You may cite this article as: Bai Y, Xie XR, Hou Y, Zhang YD, Shi HB, Wu CJ. Texture analysis enhances diagnostic accuracy of lesions scored as 5 in the Prostate Imaging Reporting and Data System in magnetic resonance imaging. *Diagn Interv Radiol.* November 2025 DOI: 10.4274/dir.2025.253640 [Epub Ahead of Print].

Advances in magnetic resonance imaging (MRI) have substantially enhanced the detection and diagnosis of prostate cancer (PCa).[1-4] The introduction of the Prostate Imaging Reporting and Data System (PI-RADS)[5] has established a crucial communication bridge between radiologists and clinicians. However, a notable issue with PI-RADS scores of 4 and 5 (considered high-risk lesions) is the high rate of false positives.[6,7] Notably, 15%–35% of these high-risk lesions are histologically benign,[8] and false-positive results lead to unnecessary biopsies,[9,10] which are invasive procedures that carry risks of complications and can erode the trust between clinicians and radiologists. The PI-RADS scoring system,[11,12] mainly based on signal intensity, may not fully capture the pathological changes in lesions.

Previous studies have revealed that among lesions with a PI-RADS score of 4 or 5 in the prostate, 14.8% (27/182) are benign, with 81.5% (22/27) of these benign cases diagnosed as prostatitis.[13] Studies have identified that apparent diffusion coefficient (ADC) values can help reduce false positives in PI-RADS 4 and 5 lesions.[14] However, research has not fully explored the imaging data, and the effectiveness of reducing false positives is limited. The development of radiomics has brought new advancements to the diagnosis of PCa.[15] Studies have demonstrated that radiomics can be used to differentiate the malignancy of PCa and distinguish clinically significant PCa with PI-RADS scores of 4 and 5.[16] However, radiomics faces several challenges, such as poor model generalizability, lack of biological interpretability, and high computational costs. Texture analysis is an essential component of radiomics and plays a crucial role in medical image analysis. By quantifying grayscale patterns and intensity variations in images, texture analysis provides deep insights into tissue heterogeneity and pathological features. This method has demonstrated substantial diagnostic efficacy in various medical applications, particularly in tumor detection and grading.[17] Research has indicated that texture analysis can be used to distinguish between benign and malignant diseases and to assess the malignancy of PCa.[18] However, this approach has not been applied to detecting lesions with PI-RADS scores of 5. This study aims to use quantitative imaging biomarkers to differentiate between cancerous and non-cancerous lesions with PI-RADS 5 scores, exploring their diagnostic accuracy.

Main points

- Texture analysis of apparent diffusion coefficient (ADC) maps enhances differentiation of prostate cancer (PCa) from benign prostatitis in lesions scored as 5 in the Prostate Imaging Reporting and Data System (PI-RADS), reducing false positives and unnecessary biopsies.
- Age, prostate-specific antigen density, and ADC texture parameters (signal coefficient of variation, ADC percentile) are independent predictors for distinguishing prostatitis from PCa in PI-RADS 5 lesions.
- A combined model integrating clinical and ADC texture parameters achieves superior diagnostic accuracy (area under the curve 93.1%) and clinical utility for improved patient management.

Methods

Patient selection

This study was approved by the Ethics Committee of The First Affiliated Hospital of Nanjing Medical University (protocol number: 2023-SRFA-467, date: 03.14.2023), with informed consent waived due to the retrospective nature of the study. We identified consecutive patients who underwent standard pelvic MRI examination before treatment by reviewing the department database for records from the period of January 2021 to July 2024. Clinical characteristics were obtained from the patient records in our hospital. Histopathological results were verified through cognitive fusion biopsies, transurethral resection of the prostate, and radical prostatectomy. Patients with the following criteria were included: (a) no prior hormonal or radiation treatment; (b) diffusion-weighted imaging (DWI) performed on a 3.0-T MRI scanner and with unified sequence parameters; and (c) lesions with pathologically confirmed PCa or prostatitis, with MRI demonstrating at least one lesion with a diameter ≥1.5 cm.

Clinical and laboratory data

Demographic data included age, and clinical data included the prostate-specific antigen (PSA) level and serum white blood cell count. The prostate volume was calculated using the following formula: (maximum anteroposterior diameter) × (maximum transverse diameter) × (maximum longitudinal diameter) × 0.52. PSA density (PSAD) was calculated by dividing the PSA level by the prostate volume.

Magnetic resonance imaging acquisition

All patients underwent a standardized prostate examination using 3.0-T MRI (Verio/Skyra, Siemens, Erlangen, Germany; u770, United Imaging, Shanghai, China) related to the probability of subsequent PSA progression (26), which complied with the PI-RADS guidelines. The multi-parametric MRI protocol included the following: (1) T2-weighted images on axial, sagittal, and coronal planes; (2) DWI on the axial plane with automatically generated ADC maps; and (3) T1-weighted sequences on axial planes with and without fat saturation. The MRI protocol technical details are listed in Table 1.

Imaging and histological correlation

The pathological results were taken as the "gold standard." The biopsy method used was transperineal prostate biopsy guided by the fusion of ultrasound and MR, and the biopsy was completed by experienced urologists. The surgical methods included transurethral prostatectomy and radical prostatectomy. The prostate samples obtained through the above methods were uniformly processed and sent to the pathology department for diagnosis. A genitourinary pathologist with 10 years of experience in genitourinary histopathology reviewed all the sample sections. Pathological diagnosis was divided into benign and malignant. Benign lesions included benign prostatic hyperplasia, prostatitis, abscess, and normal prostate tissue. Cases of PCa were graded according to the 2005 International Society of Urological Pathology Modified Gleason Grading System. Malignant lesions were further classified into Gleason score (GS) pathological grades: GS = 3 + 3, 3 + 4, and 4 + 3 and GS ≥ 4 + 4.

Texture analysis

All data were transferred in Digital Imaging and Communications in Medicine format. The region of interest (ROI) was manually delineated slice by slice along the boundaries of the tumor by one radiologist (8 years of clinical experience in prostate imaging), and the segmentations were cross-checked by another two experienced genitourinary specialist radiologists. FireVoxel (CAI2R, New York, NY, USA),[19] was used for the three-dimensional segmentation of the prostate lesions. Since PI-RADS 5 lesions all have a diameter >1.5 cm, we only selected the largest main lesion for each patient. First order and geometrical features were automatically extracted by FireVoxel. Based on histogram analysis, the following parameters were derived from the ADC

Table 1. Prostatic magnetic resonance imaging parameters of the 3.0-T scanner

Parameters	Imaging sequence		
	T2WI	T1WI	DWI
Repetition time (msec)	6.000	600	6.000
Echo time	105	24	82
Field of view (cm^2)	22	22	22
Matrix	384 × 384	384 × 384	128 × 128
Section thickness (mm)	3.5	3.5	3.5
Flip angle (degree)	110	90	90
b value (sec/mm^2)	…	…	0, 500, 1,000, and 1,500
Number of slices	25	23	23
Number of averages	2	2	2
Bandwidth/pixel	180	180	2.060
Parallel factors	2	2	2
Acquisition time (min)	3:46	3:30	3:48

T2WI, T2-weighted imaging; T1WI, T1-weighted imaging; DWI, diffusion-weighted imaging.

map: (a) minimum; (b) maximum; (c) mean; (d) kurtosis, which is the degree of peakedness of a distribution; (e) skewness, which is a measure of the degree of asymmetry of a distribution; (f) entropy, which quantifies the randomness of the gray-level distribution in an image, with higher values indicating a more dispersed and complex distribution of gray-level values; (g) coefficient of variation (COV), which quantifies the relative variability of pixel values, normalized by the mean intensity, making it useful for comparing heterogeneity across different images or ROIs; and (h) variance, which quantifies the dispersion of pixel values around the mean in the ADC, with greater variance reflecting increased tissue heterogeneity. For the cumulative histogram, the 25th, 50th, and 75th percentiles of the tumor ADC were derived (the nth percentile is the point at which n% of the voxel values that form the histogram are found to the left).

Statistical analysis

MedCalc Statistical Software, version 23.0.8 (MedCalc Software Ltd, Ostend, Belgium) was used for statistical analysis, with $P < 0.05$ considered statistically significant. The PI-RADS 5 lesions were divided into a PCa group and an inflammation group based on the pathological results. The Shapiro–Wilk and Kolmogorov–Smirnov tests were used to test the normal distribution of measurement data, and the Levene test was used to test the homogeneity of variance of measurement data. According to the test results, the normal distribution data were expressed as mean ± standard deviation (SD), the skewed distribution data were expressed as the median [upper and lower quartile (M (Q1, Q3))], and the measurement data were expressed as n (%).

Univariate and multivariate analyses were used to screen the independent risk factors for identifying inflammation and PCa in patients with PI-RADS 5 scores. If two parameters were highly correlated (e.g., PSA and PSAD, $|r| > 0.7$), the variable with greater clinical significance or a smaller *P* value in the univariate analysis was retained. The independent risk factors were combined to establish clinical ADC texture and combined models; the receiver operating characteristic (ROC) curve was drawn for the different screened models. The efficacy of different factors and models in differentiating PCa from inflammation in PI-RADS 5 lesions was evaluated. The area under the ROC curve (AUC) was used for quantification. Diagnostic sensitivity (SEN), specificity (SPE), positive predictive value (PPV), and negative predictive value (NPV) were calculated at the cut-off point with the largest Youden index. To perform decision curve analysis, R version 3.5.1 was used; this evaluates the clinical utility of the diagnostic models by assessing the net benefit of using the models to guide clinical decisions.

To evaluate the internal validity and predictive performance of the combined model, bootstrap resampling was used to generate 1,000 random samples with replacements (Python 3.13, with the sklearn.metrics and matplotlib.pyplot libraries). The ROC curve and its confidence interval (CI) were generated by calculating the mean and 95% CI of the bootstrap sample area under the curve (AUC) as well as the mean and 95% CI (SD multiplied by 1.96) of the interpolated true positive rate. This method provides a robust estimate of model performance and quantifies the uncertainty from the limited sample.

Results

Patient and lesion characteristics

The process of patient exclusion and inclusion is shown in Figure 1. A total of 189 patients were finally included, with a total of 189 tumor foci with a diameter > 1.5 cm detected in histological findings. Of the included lesions, 108 (57.1%) originated in the peripheral zone (PZ), 54 (28.5%) in the transition zone (TZ), and the remaining 27 (14.3%)in both the PZ and TZ. The median prostate volume was 27.5 mL (33.5–49.2 mL). The clinical characteristics of the patients and the tumor foci ROIs are summarized in Table 2. Representative MRI images and ADC histograms of the PCa and prostatitis cases are shown in Figures 2 and 3.

Clinical apparent diffusion coefficient texture parameters for predicting prostatitis from PI-RADS 5 lesions

Univariate and multivariate analyses were conducted to identify independent risk factors for differentiating inflammation in PI-RADS 5 lesions. Based on the clinical data, the results showed that age [odds ratio (OR): 1.081 (95% CI: 1.017–1.149)] and PSAD [OR: 35.540 (95% CI: 3.534–357.449)] are independent risk factors for diagnosing prostatitis. Based on texture feature data from whole-tumor ADC image analysis, ADC percentage values are independent risk factors for predicting prostatitis in PI-RADS 5 lesions (OR: 0.983–0.998), and signal COV has the highest OR value [OR: 1.587.241.411 (95% CI: 3.431–7.342 E + 11)] (Table 3). In these predictive parameters, age, PSAD, and signal COV are positively correlated with the prediction outcome, whereas the other variables show a negative correlation.

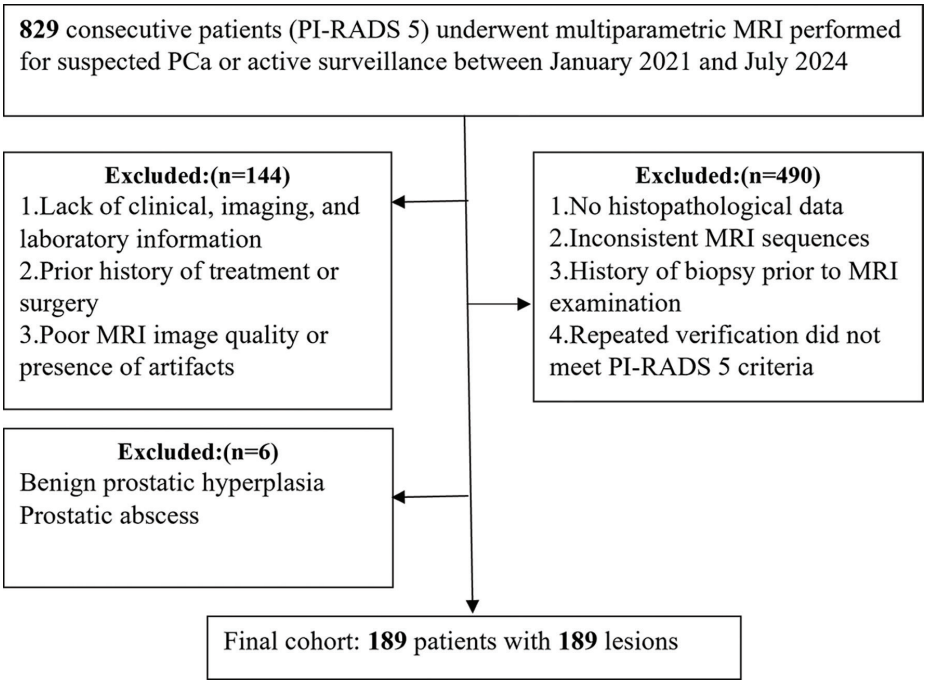

Figure 1. Flowchart of patient exclusion and inclusion. PI-RADS, Prostate Imaging Reporting and Data System; MRI, magnetic resonance imaging; PCa, prostate cancer.

Model diagnostic performance

Table 4 and Figure 4A demonstrate the diagnostic efficacy of different diagnostic models. Age and PSAD were integrated into the clinical model with diagnostic efficacy as follows: AUC of 84.6%, SEN of 97.4%, SPE of 16.0%, PPV of 95.7%, and NPV of 25.1%. The ADC texture model includes two parameters: the ADC median and signal COV. The diagnostic efficacy of this model is as follows: AUC of 86.5%, SEN of 88.1%, SPE of 44.4%, PPV of 96.8%, and NPV of 16.4%. The combined model shows a significant improvement in diagnostic performance compared with the two models mentioned above. The diagnostic efficacy is as follows: AUC of 93.1%, SEN of 98.7%, SPE of 60.0%, PPV of 97.9%, and NPV of 71.6%. There was no significant difference in diagnostic performance between the ADC texture model and clinical model (P = 0.7697). The decision curve showed that when the threshold was between 0.1 and 0.8 (Figure 4B), the combined model obtained significant clinical benefits when deciding whether to perform a biopsy. The bootstrap results showed that the performance of the combined model was robust [93.2% (95% CI: 85.6%–98.6%); Figure 5] in internal validation and superior to either the clinical model or the ADC texture model.

Discussion

The present study determined that texture analysis of ADC MRI combined with clinical parameters significantly improved the differentiation of prostatitis from PCa in PI-RADS 5 lesions. Improving the PPV of PI-RADS 5 lesions can potentially reduce unnecessary biopsies and the associated patient anxiety and morbidity. It might also lead to more appropriate treatment strategies based on a more accurate diagnosis.

Previous studies have demonstrated that PSAD identifies significant differences between prostatitis and PCa[20] and is significantly more effective than PSA in differentiating between benign and malignant histology. Integration of PSAD into decision-making for prostate biopsy may facilitate improved risk-adjusted care.[21-23] These findings are consistent with those of the present study. However, after using simple clinical parameters to build a prediction model, the AUC of the clinical model was significantly lower than that of the model constructed using ADC texture analysis, demonstrating the limitations of PSAD in identification. In addition, MRI not only measures prostate volume but also extracts texture features from ADC maps, making it a key supplementary source of data beyond clinical indicators. We found that in PI-RADS 5 lesions, the ADC parameters of the tumor were significantly lower than those of the inflammation group, which is consistent with previous studies.[24,25] However, our study only focused on PI-RADS 5 lesions, whereas other studies did not differentiate lesion PI-RADS scores; therefore, the numerical differences were greater than in this study. The narrowed data difference reflects the difficulty of the accurate diagnosis of PI-RADS 5 lesions and reflects the inadequacy of the PI-RADS scoring system, which is based on subjective qualitative evaluation of MRI. This reflects the importance of quantitative indicators for accurate diagnosis of prostate lesions, which may be of reference value for the future development of PI-RADS. In our study, there was no significant difference in histogram skewness, histogram kurtosis, or histogram entropy. This is inconsistent with previous findings and may be related to the small number of samples we included, especially the small number of prostate inflammation cases.

The study by Cheng et al.[26] found that combining clinical parameters and ADC values improved the PPV of PI-RADS 5 lesions, which is similar to our results, but they used the ADC mean and minimum without texture analysis to fully explore the possible morphological differences between PCa and inflammation. The study by Bonaffini et al.[16] used radiomics to distinguish PCa from non-cancer cases. However, with the deepening of radiomics research, it was found that the spatial resolution of MRI is still far behind that of computed tomography, and prostate lesions are usually small. Smaller ROIs may not fully utilize the advantages of radiomics, which, in turn, affects repeatability and limits interpretability. Texture analysis goes beyond simple visual inspection and provides objective measures of tissue heterogeneity. Therefore, our expectation is that texture analysis can help distinguish between tumor and non-tumor PI-RADS 5 lesions. The results of our study validate our assumptions.

Based on previous research evidence, the findings of this study may be associated with the corresponding pathophysiological changes. Although PCa and prostate inflammation show a decrease in ADC signal, the mechanisms of the two are significantly different. The mechanism of ADC decrease in PCa is mainly caused by the increase in cell density per unit of volume caused by abnormal tumor proliferation,[27-29] which restricts the diffusion of water molecules between cells. Inflammation is related to cell infiltration in the acute phase and fibrous repair in the chronic phase.[28] Compared with the significant decrease in tumor ADC value, the decrease in inflammation ADC value is relatively mild. Histogram analysis of texture analysis can detect the above changes well on MRI.

The study's strengths include the use of appropriate, reasonable, and interpretable methods to perform texture analysis

Table 2. Patient and lesion characteristics

Lesions (n = 189)	Prostatitis (n = 25)	Prostate cancer (n = 164)	***P* value**
Clinical features			
Age (years)	67.7 ± 7.2	72.0 ± 8.1	0.010
PSA (ng/mL)	8.6 (5.9–17.8)	15.1 (9.8–30.2)	0.002
PSAD (ng/mL^2)	0.18 (0.12–0.39)	0.48 (0.25–0.88)	< 0.001
Prostate volume (mL)	49.8 (35.0–60.5)	32.0 (26.5–42.9)	< 0.001
WBC (×10^9/L)	6.8 (5.5–8.6)	5.9 (5.2–7.3)	0.136
Location			
PZ (n, %)	12 (11.2)	96 (88.8)	
TZ (n, %)	10 (18.9)	44 (81.1)	
PZ + TZ (n, %)	3 (12.0)	24 (88.0)	
ISUP grade group (n/%)			
1 (GS: 3 + 3)		4 (2.4)	
2 (GS: 3 + 4)		34 (20.7)	
3 (GS: 4 + 3)		70 (42.6)	
4 (GS: 8)		3 (20.7)	
5 (GS ≥ 9)		22 (13.4)	
Specimen types (n/%)			
Biopsy	16 (64.0)	34 (20.7)	
TURP	1 (4.0)	7 (4.3)	
Radical surgery + biopsy	2 (8.0)	74 (45.1)	
TURP + biopsy	6 (24.0)	21 (12.8)	
Radical surgery		28 (17.0)	

PSA, prostate-specific antigen; PSAD, prostate-specific antigen density; WBC, white blood cell; GS, Gleason score; ISUP, International Society of Urological Pathology; TURP, transurethral resection of the prostate; PZ, peripheral zone; TZ, transition zone.

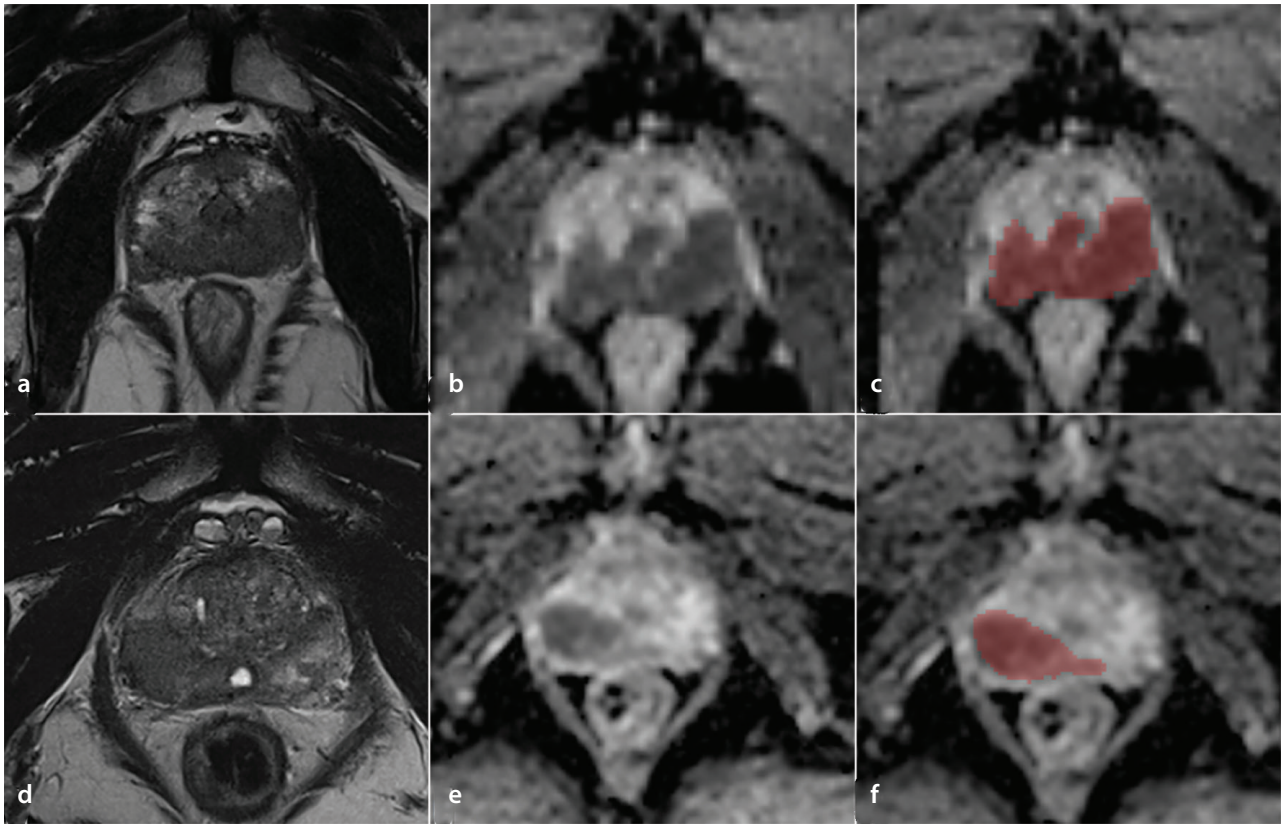

Figure 2. Magnetic resonance imaging (MRI) of prostate cancer (PCa) and prostatitis: **(a-c)** MRI images of patients with PCa; **(d-f)** MRI images of patients with prostatitis; **(a, d)** focal, low-signal lesions in the peripheral zone on T2-weighted imaging; **(b, e)** significant low signal on the apparent diffusion coefficient (ADC); **(c, f)** segmentation images on the ADC; both scored as Prostate Imaging Reporting and Data System 5.

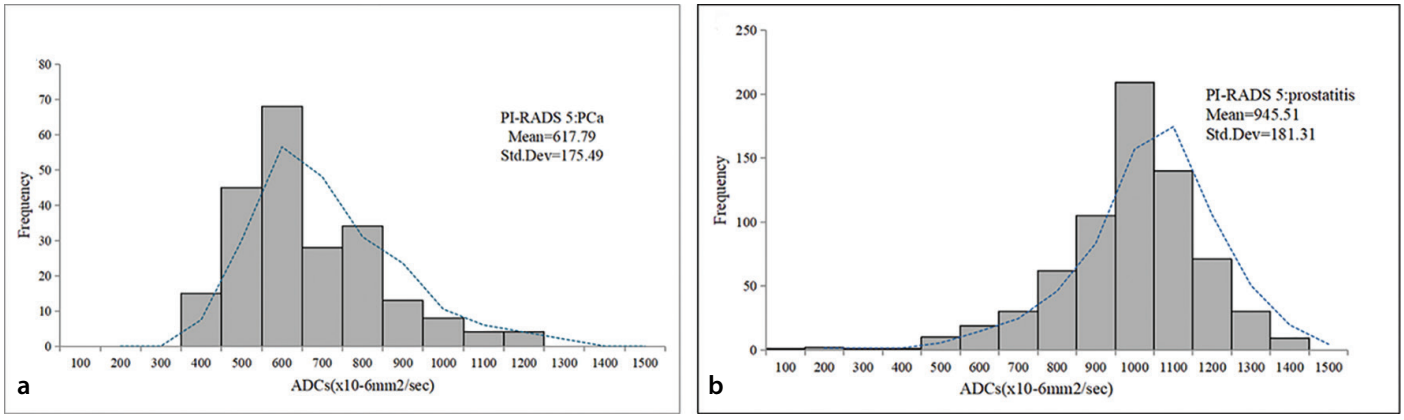

Figure 3. Comparison of whole-tumor histogram analysis of apparent diffusion coefficients (ADCs) between prostate cancer (PCa) and prostatitis: PCa foci **(a)** showing a higher relative frequency at low ADCs than **(b)** prostatitis foci, resulting in significant divergence between prostatitis and PCa at the high end of the cumulative ADC histogram. This suggests that PCa contained more pixels with low ADCs, indicating high cellularity. Std. Dev., Standard deviation.

Table 3. Clinical and apparent diffusion coefficient texture univariate and multivariate analyses

	Univariate analysis		Multivariate analysis	
Clinical	OR (95% CI)	*P* value	OR (95% CI)	*P* value
Age (years)	1.069 (1.013–1.128)	0.015	1.081 (1.017–1.149)	0.012
PSA (ng/mL)	1.053 (1.009–1.098)	0.017		
Prostate volume (mL)	0.986 (0.961–0.991)	0.002	0.990 (0.971–1.009)	0.291
WBC ($\times 10^9$/L)	0.776 (0.619–0.972)	0.028		
PSAD (ng/mL^2)	68.469 (6.074–771.759)	0.001	35.540 (3.534–357.449)	0.002
ADC texture				
Histogram skewness	1.787 (0.617–5.177)	0.457		
Histogram kurtosis	1.050 (0.701–1.570)	0.971		
Histogram entropy	0.213 (0.012–3.743)	0.246		
ADC minimum	0.990 (0.986–0.995)	< 0.001		
ADC 5%	0.983 (0.977–0.989)	< 0.001		
ADC 25%	0.986 (0.981–0.991)	< 0.001		
ADC median	0.987 (0.982–0.992)	< 0.001	0.990 (0.985–0.995)	<0.001
ADC 75%	0.989 (0.984–0.993)	< 0.001		
ADC 95%	0.992 (0.988–0.996)	< 0.001		
ADC maximum	0.998 (0.995–1.000)	0.063		
ADC mean	0.986 (0.981–0.991)	< 0.001		
Signal COV	1.520 E+11 (1,674,931.931–1.379 E + 16)	< 0.001	1,587,241.411 (3.431–7.342 E + 11)	0.032
Signal SD	1.012 (0.997–1.026)	0.084		

PSA, prostate-specific antigen; PSAD, prostate-specific antigen density; WBC, white blood cell; ADC, apparent diffusion coefficient; COV, coefficient of variation; SD, standard deviation; CI, confidence interval; OR, odds ratio.

Table 4. Diagnostic performance of different diagnostic models

	AUC (%)	SEN (%)	SPE (%)	PPV (%)	NPV (95%)	ACC
Clinical model[ab]	84.6 (78.5–89.4)	97.4 (93.6–99.3)	16.0 (4.5–36.1)	95.7 (94.8–96.3)	25.1 (8.2–55.6)	93.4 (88.8–96.5)
ADC texture model[ac]	86.5 (80.7–91.1)	88.1 (82.3–92.4)	44.4 (13.7–78.8)	96.8 (94.3–98.1)	16.4 (7.8–31.0)	85.9 (80.0–90.6)
Combined model[bc]	93.1 (88.4–96.3)	98.7 (95.5–99.8)	60.0 (38.6–78.8)	97.9 (96.6–98.7)	71.6 (38.0–91.2)	96.8 (93.1–98.8)

[a]: Clinical model vs. ADC texture model: $P = 0.7697$.
[b]: Clinical model vs. combined model: $P = 0.0038$.
[c]: ADC texture model vs. combined model: $P = 0.0812$.
AUC, area under the curve; SEN, sensitivity; SPE, specificity; PPV, positive predictive value; NPV, negative predictive value; ADC, apparent diffusion coefficient; ACC, accuracy.

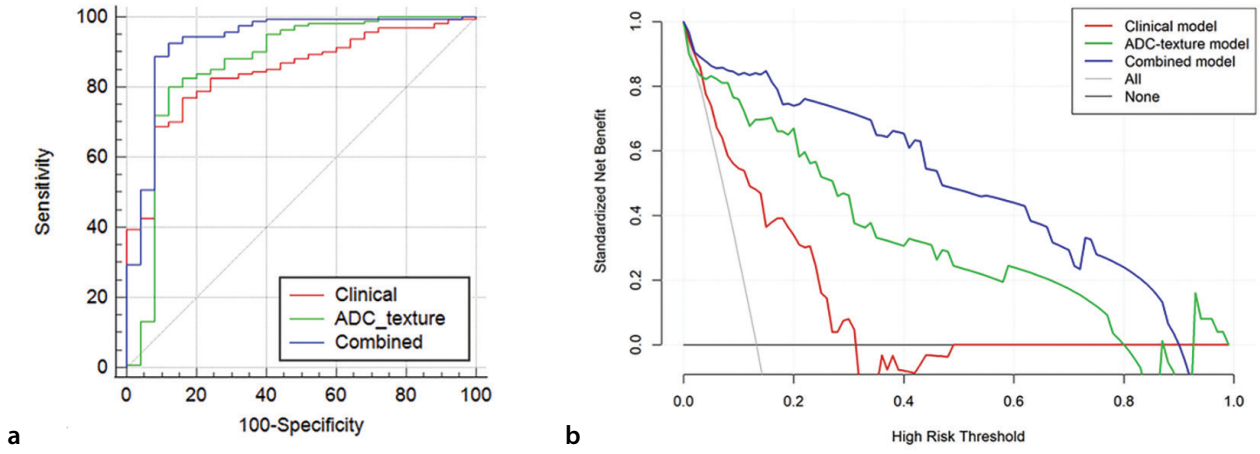

Figure 4. Receiver operating characteristic curve (ROC) and decision curve of different models: **(a)** ROC analysis demonstrates superior performance of the combined model (area under the curve: 0.931, sensitivity: 0.987, specificity: 0.600, positive predictive value: 0.979, negative predictive value: 0.716) to the apparent diffusion coefficient (ADC) texture and clinical models ($P < 0.05$). **(b)** Decision curve analysis reveals the combined model provides greater clinical net benefit across risk thresholds (0.1–0.8) than individual models.

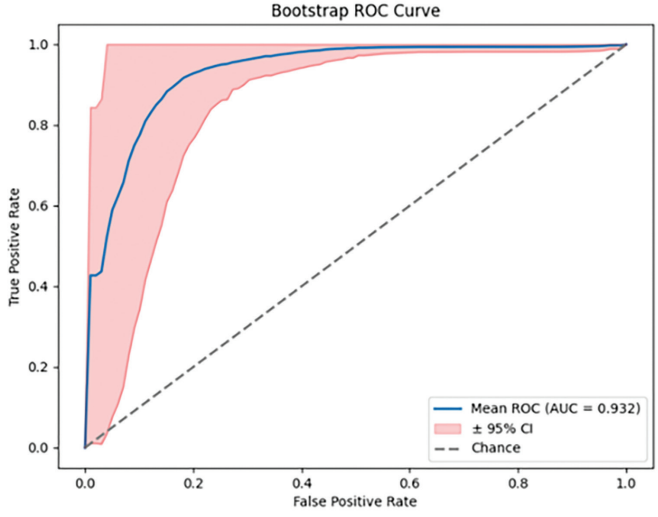

Figure 5. Internal validation. The bootstrap results demonstrated that the performance of the combined model was robust [93.2% (95% CI: 85.6%–98.6%)] in internal validation. ROC, receiver operating characteristic; AUC, area under the curve; CI, confidence interval.

for accurate diagnosis of MRI-visible lesions assigned a score of PI-RADS 5. The volume of the prostate and the lesions within it are small, the ADC spatial resolution is not high, and the organs and lesions themselves and the scanning sequence parameters limit the full play of high-throughput, multi-dimensional image analysis methods such as radiomics. The combination of texture analysis parameters and clinical indicators for prediction improves the accuracy of the diagnosis of lesions classified as PI-RADS 5. This diagnostic model not only further distinguishes the nature of lesions based on the existing PI-RADS but also serves as a supplement and improvement to PI-RADS.

From a total of 829 consecutive cases screened as PI-RADS 5 in a single center, we selected 189 cases that had complete clinical, imaging, and pathological data. These cases were closer to real-world cases. The sample size of prostatitis cases in this study is limited, which may lead to potential overfitting in the constructed model. To address this issue, the bootstrap method was employed for internal validation, ultimately verifying the diagnostic accuracy of the newly developed model.

Our study is subject to certain limitations. It is a single-center investigation with a limited sample size of prostatitis cases, and external validation has not been conducted. We plan to conduct a multi-center, large-sample study in the future. Inter-reader variability in ROI drawing, although minimized by training, is still a potential factor influencing the model's accuracy. Although the machine scanning parameters are the same, we used three different machine models from two manufacturers. Existing studies have verified that different equipment models can lead to significant inconsistencies in radiomic feature extraction; for instance, Tocilă-Mătăşel et al.[30] reported that texture features varied when acquired from different MRI scanners with different parameters. Hajianfar et al.[31] further verified that such equipment-induced variability could reduce the robustness of radiomics models in clinical applications. The impact of different machine models on texture analysis needs to be further studied, especially regarding how to mitigate its interference with the robustness of results.

In conclusion, ADC texture parameters (signal COV, ADC median), PSAD, and age are independent risk factors for distinguishing PCa and prostatitis in PI-RADS 5 lesions. The ADC texture analysis of lesions with a PI-RADS score of 5 combined with clinical parameters can effectively improve the accuracy of diagnosis to reduce unnecessary biopsies and improve patient management.

Footnotes

Conflict of interest disclosure

The authors declared no conflicts of interest.

Funding

The authors declared that they have disclosed direct or indirect affiliation or financial interests in connection with the content of this paper: NSFC 62303235 (WCJ), NSFC 82302308 (YH).

References

1. Dickinson L, Ahmed HU, Allen C, et al. Magnetic resonance imaging for the detection, localisation, and characterisation of prostate cancer: recommendations from a European consensus meeting. Eur Urol. 2011;59(4):477-494. [Crossref]
2. Murphy G, Haider M, Ghai S, Sreeharsha B. The expanding role of MRI in prostate cancer. *AJR Am J Roentgenol.* 2013;201(6):1229-1238. [Crossref]
3. Johnson LM, Turkbey B, Figg WD, Choyke PL. Multiparametric MRI in prostate cancer management. *Nat Rev Clin Oncol.* 2014;11(6):346-353. [Crossref]
4. Sciarra A, Barentsz J, Bjartell A, et al. Advances in magnetic resonance imaging: how they are changing the management of prostate cancer. *Eur Urol.* 2011;59(6):962-977. [Crossref]
5. Barentsz JO, Richenberg J, Clements R, et al. ESUR prostate MR guidelines 2012. *Eur Radiol.* 2012;22(4):746-757. [Crossref]
6. Woo S, Suh CH, Kim SY, Cho JY, Kim SH. Diagnostic Performance of Prostate Imaging Reporting and Data System Version 2 for detection of prostate cancer: a systematic review and diagnostic meta-analysis. *Eur Urol*. 2017;72(2):177-188. [Crossref]
7. Ahmed HU, El-Shater Bosaily A, Brown LC, et al. Diagnostic accuracy of multi-parametric MRI and TRUS biopsy in prostate cancer (PROMIS): a paired validating confirmatory study. *Lancet*. 2017;389(10071):815-822. [Crossref]
8. Şeref C, Acar Ö, Kılıç M, et al. Histologically benign PI-RADS 4 and 5 lesions contain cancer-associated epigenetic alterations. Prostate. 2022;82(1):145-153. [Crossref]
9. Sheridan AD, Nath SK, Aneja S, et al. MRI-ultrasound fusion targeted biopsy of prostate imaging reporting and data system version 2 category 5 lesions found false-positive at multiparametric prostate MRI. *AJR Am J Roentgenol.* 2018; 210(5):W218-W225. [Crossref]
10. Apfelbeck M, Pfitzinger P, Bischoff R, et al. Predictive clinical features for negative histopathology of MRI/Ultrasound-fusion-guided prostate biopsy in patients with high likelihood of cancer at prostate MRI: analysis from a urologic outpatient clinic. *Clin Hemorheol Microcirc.* 2020;76(4):503-511. [Crossref]
11. Turkbey B, Rosenkrantz AB, Haider MA, et al. Prostate imaging reporting and data system version 2.1: 2019 update of prostate imaging reporting and data system version 2. *Eur Urol.* 2019;76(3):340-351. [Crossref]
12. Weinreb JC, Barentsz JO, Choyke PL, et al. PI-RADS prostate imaging - reporting and data system: 2015, version 2. *Eur Urol.* 2016;69(1):16-40. [Crossref]
13. Wang X, Liu W, Lei Y, Wu G, Lin F. Assessment of prostate imaging reporting and data system version 2.1 false-positive category 4 and 5 lesions in clinically significant prostate cancer. *Abdom Radiol.* 2021;46(7):3410-3417. [Crossref]
14. Polanec SH, Helbich TH, Bickel H, et al. Quantitative apparent diffusion coefficient derived from diffusion-weighted imaging has the potential to avoid unnecessary MRI-guided biopsies of mpMRI-detected PI-RADS 4 and 5 lesions. *Invest Radiol.* 2018;53(12):736-741. [Crossref]
15. Wang J, Wu CJ, Bao ML, Zhang J, Wang XN, Zhang YD. Machine learning-based analysis of MR radiomics can help to improve the diagnostic performance of PI-RADS v2 in clinically relevant prostate cancer. *Eur Radiol.* 2017;27(10):4082-4090. [Crossref]
16. Bonaffini PA, De Bernardi E, Corsi A, et al. Towards the definition of radiomic features and clinical indices to enhance the diagnosis of clinically significant cancers in PI-RADS 4 and 5 lesions. *Cancers (Basel).* 2023;15(20):4963. [Crossref]
17. Ghalati MK, Nunes A, Ferreira H, Serranho P, Bernardes R. Texture analysis and its applications in biomedical imaging: a survey. *IEEE Rev Biomed Eng.* 2021;15:222-246. [Crossref]
18. Corsi A, De Bernardi E, Bonaffini PA, et al. Radiomics in PI-RADS 3 multiparametric MRI for prostate cancer identification: literature models re-implementation and proposal of a clinical-radiological model. *J Clin Med.* 2022;11(21):6304. [Crossref]
19. Doshi AM, Tong A, Davenport MS, et al. Assessment of renal cell carcinoma by texture analysis in clinical practice: a six-site, six-platform analysis of reliability. *AJR Am J Roentgenol.* 2021;217(5):1132-1140. [Crossref]
20. Iersel MPV, Witjes W, ROSETTE JD, Oosterhof G. Prostate-specific antigen density: correlation with histological diagnosis of prostate cancer, benign prostatic hyperplasia and prostatitis. *Br J Urol.*1995;76(1):47-53. [Crossref]
21. Wang S, Kozarek J, Russell R, et al. Diagnostic performance of prostate-specific antigen density for detecting clinically significant prostate cancer in the era of magnetic resonance imaging: a systematic review and meta-analysis. *Eur Urol Oncol*. 2024;7(2):189-203. [Crossref]
22. Wang C, Yuan L, Shen D, et al. Combination of PI-RADS score and PSAD can improve the diagnostic accuracy of prostate cancer and reduce unnecessary prostate biopsies. *Front Oncol.* 2022;12:1024204. [Crossref]
23. Stevens E, Truong M, Bullen JA, Ward RD, Purysko AS, Klein EA. Clinical utility of PSAD combined with PI-RADS category for the detection of clinically significant prostate cancer. *Urol Oncol.* 2020;38(11):846.e9-846.e16. [Crossref]
24. Nagel KN, Schouten MG, Hambrock T, et al. Differentiation of prostatitis and prostate cancer by using diffusion-weighted MR imaging and MR-guided biopsy at 3 T. *Radiology.* 2013;267(1):164-172. [Crossref]
25. Hoeks CM, Vos EK, Bomers JG, Barentsz JO, Hulsbergen-van de Kaa CA, Scheenen TW. Diffusion-weighted magnetic resonance imaging in the prostate transition zone: histopathological validation using magnetic resonance-guided biopsy specimens. *Invest Radiol.* 2013;48(10):693-701. [Crossref]
26. Cheng Y, Fan B, Fu Y, et al. Prediction of false-positive PI-RADS 5 lesions on prostate multiparametric MRI: development and internal validation of a clinical-radiological characteristics based nomogram. *BMC Urol.* 2024;24(1):76. [Crossref]
27. Koh DM, Collins DJ. Diffusion-weighted MRI in the body: applications and challenges in oncology. *AJR Am J Roentgenol.* 2007;188(6):1622-1635. [Crossref]
28. Gass A, Niendorf T, Hirsch JG. Acute and chronic changes of the apparent diffusion coefficient in neurological disorders--biophysical mechanisms and possible underlying histopathology. *J Neurol Sci.* 2001;186:S15-S23. [Crossref]
29. Herneth AM, Guccione S, Bednarski M. Apparent diffusion coefficient: a quantitative parameter for *in vivo* tumor characterization. *Eur J Radiol.* 2003;45(3):208-213. [Crossref]
30. Tocilă-Mătăşel C, Dudea SM, Iana G. Addressing multi-center variability in radiomic analysis: a comparative study of image acquisition methods across two 3T MRI scanners. *Diagnostics.* 2025;15(4):485. [Crossref].
31. Hajianfar G, Hosseini SA, Bagherieh S, Oveisi M, Shiri I, Zaidi H. Impact of harmonization on the reproducibility of MRI radiomic features when using different scanners, acquisition parameters, and image pre-processing techniques: a phantom study. *Med Biol Eng Comput*. 2024;62(8):2319-2332. [Crossref]